International Journal of Engineering Research and Development
e- ISSN: 2278-067X, p-ISSN: 2278-800X, www.ijerd.com
Volume 21, Issue 6 (June 2025), PP 69-83

Influence of Cooling Systems on a Dual-Fluid CPVT Solar Concentrator (Water and Air)

PASERA Joanès Keneddy[1],HARITHI BEN Daoud Ben Attoumane[2],
DONA Victorien Bruno[3]

[1]*Ph.D. student, Laboratory of Applied Physics and Renewable Energies (LPADER), EcoleDoctoraleGénie du Vivant et Modélisation (EDGVM), University of Mahajanga, Madagascar;*
[2]*Ph.D. student, Laboratory of Applied Physics and Renewable Energies (LPADER), EcoleDoctoraleGénie du Vivant et Modélisation (EDGVM), University of Mahajanga, Madagascar;*
[3]*Professor, Laboratory of Applied Physics and Renewable Energies (LPADER), EcoleDoctoraleGénie du Vivant etModélisation (EDGVM), University of Mahajanga, Madagascar;*
Corresponding Author:PASERA JoanèsKeneddy;

Abstract: *This study focuses on optimizing the energy performance of a dual-fluid (water and air) photovoltaic-thermal (PVT) cogeneration system integrated with a solar concentrator (dual-fluid CPVT). This innovative system aims to maximize solar energy utilization by balancing thermal and electrical outputs through efficient cooling management, while being adapted to the specific climatic conditions of Mahajanga. The reflectors capture and concentrate solar radiation, increasing the irradiation on the absorber and reducing reflective losses. This intensified solar flux significantly enhances the system's overall energy efficiency. Furthermore, the integration of fins and the simultaneous use of both fluids improve the cooling of photovoltaic cells and heat transfer to the air. However, this configuration slightly limits heat recovery by the water, necessitating the optimization of both external and internal parameters. A one-dimensional dynamic numerical model was developed and simulated using MATLAB with the Runge-Kutta method. Analysis of the results demonstrates that tuning the number and characteristics of the fins, as well as the mass flow rates of the fluids (water and air), enables an optimal balance between electrical generation and thermal recovery. This approach ensures stable electricity production, efficient domestic hot water generation, and the provision of hot air suitable for drying applications. Through rigorous modeling and advanced simulations, this study makes a significant contribution to the development of hybrid photovoltaic-thermal systems, offering promising prospects for enhanced solar energy utilization within the framework of a sustainable energy transition.*

Keywords: *Solar irradiation, Dual-fluid PVT system, Fins, Mass flow rate, Solar concentrator, Performance*

Date of Submission: 06-06-2025 Date of acceptance: 16-06-2025

I. Introduction

Hybrid photovoltaic-thermal (PVT) collectors represent an innovative technology that enhances solar energy conversion by simultaneously generating electricity and thermal energy. However, the overheating of photovoltaic (PV) cells remains a major challenge, leading to a significant reduction in electrical efficiency [1]. To address this issue, the implementation of effective cooling strategies is essential to optimize heat dissipation and improve the overall performance of the system.

Various studies have explored different configurations of PVT systems integrating a compound parabolic concentrator (PVT-CPC) and using water-based heat transfer fluids. For instance, Tripathi and Tiwari (2017) and DeepaliAtheaya et al. (2016) investigated systems with flat-plate and tubular absorbers [2,3]. Other works by Ahed Hameed Jaaz et al. (2010) and Mekadem and Mellouki (2022) focused on water jet cooling to enhance thermal management [4,5]. Additionally, Wenzhi Cui et al. proposed a quasi-CPC concept to optimize solar radiation capture [6]. In parallel, several studies have examined air-based PVT systems operating under solar concentration. Notably, Tabet Ismail (2016) analyzed a system using flat reflectors [7], while our study focused on the development of a PVT-CCPH system integrating a cylindrical-parabolic concentrator and a heliostat [8,9].

The proposed hybrid CPVT dual-fluid solar concentrator system combines the principles of water-based and air-based CPVT technologies within a single collector. By integrating two heat transfer fluids (water and air) simultaneously, the system allows for optimized thermal management, promoting enhanced heat extraction while effectively controlling the temperature of PV cells exposed to high solar concentration [10].

Optimizing such PVT systems is particularly relevant in high solar irradiance regions such as Mahajanga (Madagascar), where solar energy represents an abundant resource. To fully harness this potential, integrating a concentrator like the compound parabolic cylindrical collector into a dual-fluid PVT system offers an innovative solution. This concentrator focuses solar radiation without requiring complex tracking mechanisms, ensuring improved energy distribution across the PVT receiver while reducing hot spots and enhancing both thermal and electrical performance [6,11]. However, the increased solar concentration results in higher PV cell temperatures, making efficient thermal management critical.

In this context, the present study aims to analyze and optimize the performance of a dual-fluid CPVT system by evaluating the influence of fin characteristics (number, height, thickness) and the mass flow rates of the fluids (air and water) on thermal and electrical performance. Particular attention is given to the interaction between the two fluids to simultaneously optimize PV cell cooling and heat recovery. The objective is to determine the optimal fin configuration and fluid mass flow rates that maximize the system's energy efficiency. Final recommendations are provided to enhance system design and ensure an optimal balance between electrical and thermal performance.

To this end, an innovative cooling system has been designed, incorporating double aluminum absorbers (one of which is finned), parallel tubes, and two heat transfer fluids. The recovered hot water can be used for domestic heating, while the hot air is suitable for agricultural drying applications. The study is based on MATLAB modeling to assess cooling effectiveness and optimize parameters in order to maximize the energy yields of the hybrid system.

II. Material And Methods

2.1 Description of the examined system configuration

The dual-fluid hybrid PVT collector consists of multiple distinct layers, including a glass cover, photovoltaic (PV) cells, an EVA (ethylene-vinyl acetate) film, a Tedlar backsheet, an upper absorber with fins, a tube carrying the heat transfer fluid (water), an air-based heat transfer layer, a lower absorber, and thermal insulation.The collector is positioned between two symmetrical compound parabolic cylindrical concentrators, enabling it to harness both direct solar radiation and the radiation reflected by the concentrators. These reflectors play a crucial role in capturing and focusing solar radiation to intensify the irradiation received by the dual-fluid PVT collector, thereby improving its overall energy efficiency.

The photovoltaic cells generate electricity, while part of the incident solar energy is converted into thermal energy. The water and air flowing beneath the PV module absorb this heat, helping to reduce the temperature of the PV cells. On one hand, the heated water can be stored for thermal applications such as space heating or domestic hot water production. On the other hand, the hot air can be directed into a drying chamber using a fan, ensuring uniform heat distribution and enhancing the efficiency of the drying process for agricultural or other products [10].

The water-based PVT collector consists of the following layers: glass, PV cells, EVA film, Tedlar, absorber, parallel tubes, heat transfer fluid (water), and thermal insulation. In contrast, the configuration of the air-based PVT collector, as presented in our studies [11,12], includes specific design adaptations to accommodate air flow circulation.

Figures 1 and 2 below illustrate the configuration of a hybrid solar CPVT collector using water and CPVT using air [10].

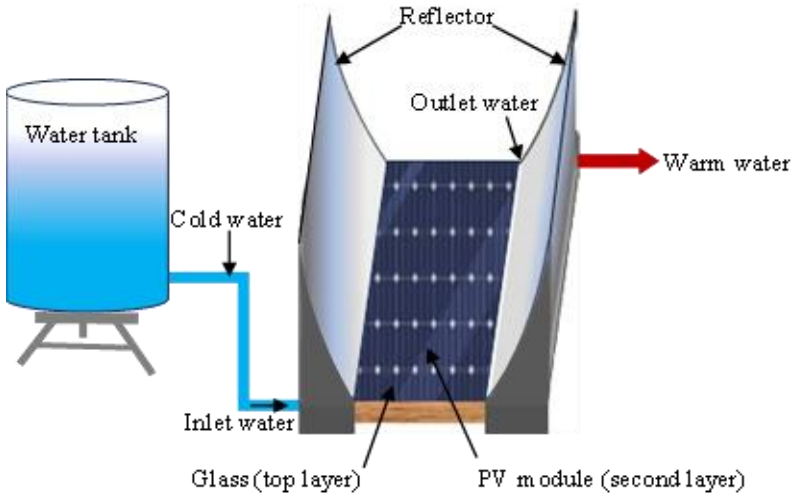

Figure 1: Schematic diagram of a water-based CPVT hybrid solar collector

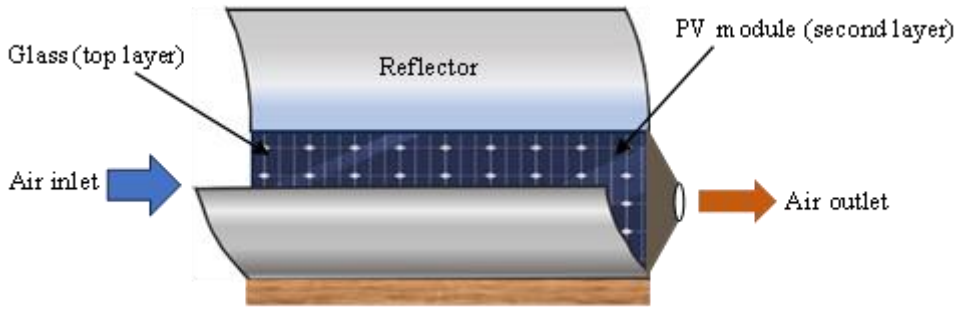

Figure 2: Schematic of an air-based hybrid CPVT solar collector

A cross-section of a dual-fluid hybrid CPVT solar collector is shown in figure 3 [9,10,12,13,14].

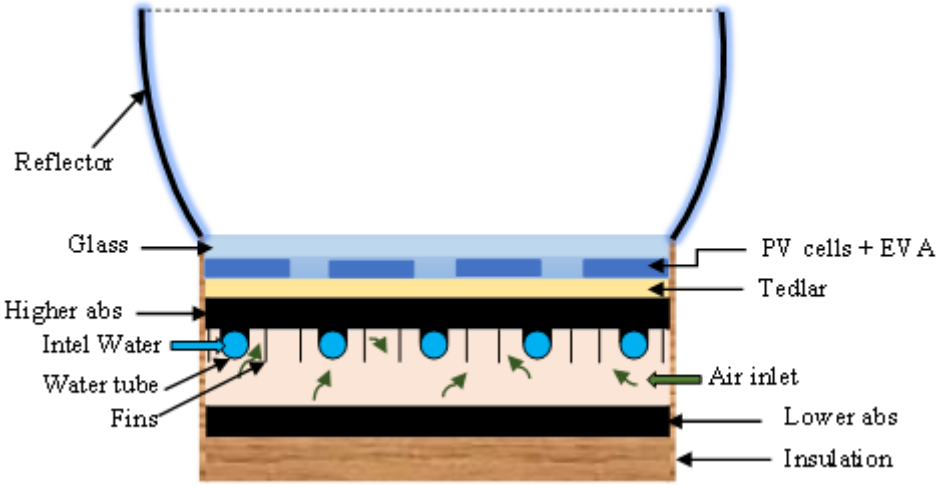

Figure 3: Front view sketch of bi-fluid CPVT system

2.2Mathematical modeling

2.2.1Study hypothesis

The mathematical models used to simulate the dual-fluid CPVT system are based on the following assumptions [9,10,15]:

- The sky can be assimilated to a black body with an equivalent temperature calculated;
- Heat transfer is considered to be one-dimensional through the layers of the system;
- The ambient temperature is the same around the sensor;
- The floor temperature is taken to be equal to the ambient temperature;
- EVA's transmission coefficient is 100%;
- The ohmic losses of the solar cells are neglected;
- The mass flow rate is uniform in the air layer duct;
- Fluid flow in the tubes is assumed to be uniform;
- The wind speed on the face of the collector is assumed to be constant;
- The thermo-physical properties of water and air vary with temperature;
- The thermal and geometric properties of the two absorbers are equal;
- The thermal properties of the fins and tubes are equal to those of the absorber;
- The effect of shading and dust on the collector is negligible;

2.2.2Equation the system

The mathematical model of the dual-fluid CPVT system is formulated based on energy balance equations applied to the individual control volumes, as presented in references [5,7,9,10,12,13,14,15,16]:

Node 1 : outer face of glass

$$m_g Cp_g \left(\frac{dT_{g,ext}}{dt}\right) = A_g G_i C - h_{g-a}^{conv} A_g \left(T_{g,ext} - T_a\right) - h_g^{cond} A_g \left(T_{g,ext} - T_{g,int}\right) - h_{g-sky}^{rad} A_g \left(T_{g,ext} - T_{sky}\right) \quad (1)$$

Node 2 :inner face of glass pane

$$m_g Cp_g \left(\frac{dT_{g,int}}{dt}\right) = A_g \alpha_g G_i C + h_g^{cond} A_g \left(T_{g,ext} - T_{g,int}\right) - h_{g-cel}^{cond} A_g \left(T_{g,int} - T_{cel}\right) \quad (2)$$

Node 3 :PV cell

$$m_{cel} Cp_{cel} \left(\frac{dT_{cel}}{dt}\right) = A_{cel} \tau_g \alpha_{cel} G_i C + h_{g-cel}^{cond} A_{cel} \left(T_{g,int} - T_{cel}\right) - h_{cel-ted}^{cond} A_{cel} \left(T_{cel} - T_{ted}\right) - Q_{élec} \quad (3)$$

Node 4 : tedlar layer

$$m_{ted} Cp_{ted} \left(\frac{dT_{ted}}{dt}\right) = h_{cel-ted}^{cond} A_{ted} \left(T_{cel} - T_{ted}\right) - h_{ted-absh}^{cond} A_{ted} \left(T_{ted} - T_{absh}\right) \quad (4)$$

Node 5 :top absorber layer

$$\begin{aligned} m_{abs} Cp_{abs} \left(\frac{dT_{absh}}{dt}\right) = {} & h_{ted-absh}^{cond} A_{abs} \left(T_{ted} - T_{absh}\right) - h_{absh-air}^{conv} A_{absh-air} \left(T_{absh} - T_{air}\right) - U_{fin} \left(T_{absh} - T_{air}\right) \\ & - h_{absh-tube}^{cond} A_{absh-tube} \left(T_{absh} - T_{tube}\right) - h_{absh-absl}^{rad} A_{absh-absl} \left(T_{absh} - T_{absl}\right) \end{aligned} \quad (5)$$

With [10]: $U_{fin} = h_{absh-air}^{conv} . \eta_{fin} . A_{absh-air}$ (6)

$$\eta_{fin} = \frac{\tanh\left(L_c \cdot \sqrt{\frac{P.h_{fin}^{conv}}{\lambda_{fin} e_{fin}}}\right)}{L_c \cdot \sqrt{\frac{P.h_{fin}^{conv}}{\lambda_{fin} . e_{fin}}}}, \quad A_{absh-air} = N.\left(2.H_{fin} . L_c\right) + A_{absh} + A_{tube}, \quad L_c = L + \frac{e_{fin}}{2} \text{ et } P = 2\left(L + e_{fin}\right) \quad (7)$$

Where : $A_{absh-air}$, L_c, P and e_{fin} are respectively the total available area, corrected length, perimeter and thickness of a fin.

Node 6 : tube layer

$$\begin{aligned} m_{tube} Cp_{tube} \left(\frac{dT_{tube}}{dt}\right) = {} & h_{absh-tube}^{cond} A_{absh-tube} \left(T_{absh} - T_{tube}\right) - h_{tube-wat}^{conv} A_{tube-wat} \left(T_{tube} - T_{wat}\right) \\ & - h_{tube-air}^{conv} A_{tube-air} \left(T_{tube} - T_{air}\right) - h_{tube-absl}^{ray} A_{tube-absl} \left(T_{tube} - T_{absl}\right) \end{aligned} \quad (8)$$

Node 7 :heat transfer fluid water

$$m_{wat} Cp_{wat} \left(\frac{dT_{wat}}{dt}\right) = h_{tube-wat}^{conv} A_{tube-wat} \left(T_{tube} - T_{wat}\right) - \dot{m}_{wat} Cp_{wat} \left(T_{wat,out} - T_{wat,int}\right) \quad (9)$$

Node 8:heat transfer fluid air

$$\begin{aligned} m_{air} Cp_{air} \left(\frac{dT_{air}}{dt}\right) = {} & h_{absh-air}^{conv} A_{absh-air} \left(T_{absh} - T_{air}\right) + h_{air-absl}^{conv} A_{air-absl} \left(T_{absl} - T_{air}\right) \\ & + h_{tube-air}^{conv} A_{tube-air} \left(T_{tube} - T_{air}\right) + U_{fin} \left(T_{absh} - T_{air}\right) - \dot{m}_{air} Cp_{air} \left(T_{air,out} - T_{air,int}\right) \end{aligned} \quad (10)$$

Node 9 :lower absorber layer

$$\begin{aligned} m_{absl} Cp_{absl} \left(\frac{dT_{absl}}{dt}\right) = {} & h_{air-absl}^{conv} A_{air-absl} \left(T_{air} - T_{absl}\right) + h_{absh-absl}^{rad} A_{absh-absl} \left(T_{absh} - T_{absl}\right) \\ & + h_{tube-absl}^{rad} A_{tube-absl} \left(T_{tube} - T_{absl}\right) - h_{absl-is}^{cond} A_{absl-is} \left(T_{absl} - T_{is,int}\right) \end{aligned} \quad (11)$$

Node 10 : inner face of the insulation

$$m_{is} Cp_{is} \left(\frac{dT_{is,int}}{dt}\right) = h_{absl-is}^{cond} A_{is} \left(T_{absl} - T_{is,int}\right) - h_{is}^{cond} A_{is} \left(T_{is,int} - T_{is,ext}\right) \quad (12)$$

Node 11 :outer face of the insulation

$$m_{is}Cp_{is}\left(\frac{dT_{is,ext}}{dt}\right)=h_{is}^{cond}A_{is}\left(T_{is,int}-T_{is,ext}\right)-h_{is-a}^{conv}A_{is}\left(T_{is,ext}-T_{a}\right)-h_{is-sol}^{rad}A_{is}\left(T_{is,ext}-T_{sol}\right) \quad (13)$$

2.2.3Heat exchange coefficients

❖ **Conductive heat transfer coefficient**

In general, the conductive heat transfer coefficient between two layers of adjacent components m_i and n_i is given by the empirical relationship as follows [8,12,13]:

$$h_{m_i-n_i}^{cond}=\left(\frac{e_{m_i}}{\lambda_{m_i}}+\frac{e_{n_i}}{\lambda_{n_i}}\right)^{-1} \quad (14)$$

❖ **Coefficient of radiant heat exchange** [8,12,13]

The radiative exchange coefficient is calculated using empirical formulas as follows :

$$h_{g-sky}^{rad}=\varepsilon_g.\sigma.\left(T_{g,ext}+T_{sky}\right)\left(T_{g,ext}^2+T_{sky}^2\right) \quad (15)$$

$$h_{mi-ni}^{rad}=\sigma\frac{\left(T_{mi}+T_{ni}\right)\left(T_{mi}^2+T_{ni}^2\right)}{\left(\frac{1}{\varepsilon_{mi}}\right)+\left(\frac{1}{\varepsilon_{ni}}\right)-1} \quad (16)$$

Where : $\sigma=5,67\times10^{-8}$, Stephan Boltzmann's constant ;

$T_{sky}=0,0552.\left(T_a\right)^{1,5}$, the sky temperature is given by the Swinbank relation. (17)

With : $T_a=\left[\frac{T_{a\,max}-T_{a\,min}}{2}\right].\cos\left[\frac{(TSV-12).\pi}{12}\right]+\left[\frac{T_{a\,max}+T_{a\,min}}{2}\right]$, ambienttemperature (18)

❖ **Convective heat transfer coefficients** [8,12,13,14]

The Mac Adams correlation was used to determine the heat exchange between the glass and the environment :

$h_{v-a}^{conv}=5.6+3.8\times V_{vent}$, where : V_{vent} is the wind speed. (19)

Convective heat exchange coefficients are calculated by empirical correlations using the Nusselt number:

$$h_{air}^{conv}=\frac{Nu_{air}\lambda_{air}}{D_h}\ \text{et}\ h_{wat}^{conv}=\frac{Nu_{wat}\lambda_{wat}}{D_{int}} \quad (20)$$

Heat transfer between absorber and fluid :

$$h_{abs-air}^{conv}=\left(\frac{e_{abs}}{\lambda_{abs}}+\frac{1}{h_{air}^{conv}}\right)^{-1} \quad (21)$$

The physical properties of air are assumed to vary linearly with temperature, in accordance with the specific expressions established by Ebrahim and Alfege [12,15] :

- Massdensity: $\rho_{air}=1.1774-0.000359\times T_{air}$;(22)
- Specificheat : $Cp_{air}=\left[1.0057+0.000066\times T_{air}\right]\times1009$;(23)
- Thermal conductivity: $\lambda_{air}=0.02624+0.0000758\times T_{air}$; (24)
- Dynamicviscosity: $\mu_{air}=\left[1.983+0.00184\times T_{air}\right]\times10^{-5}$. (25)

In our case, the Nusselt number is calculated according to the flow regime, which is expressed by the following equations [9,17] :

- For laminar flow $\left(Re_{air}<2300\right)$

$$Nu_{air}=N_{\infty}+\frac{0.0019\times\left[Pr_{air}\cdot Re_{air}\cdot D_h/L\right]^{1.71}}{1+0.00563\times\left[Pr_{air}\cdot Re_{air}\cdot D_h/L\right]^{1.17}}\text{ , (Heaton'sempiricalcorrelation)} \quad (26)$$

With: $N_{\infty} = 5.4,\ Pr_{air} = 0.7$

- For transient flow $\left(2300 \le Re_{air} \le 6000\right)$

$$Nu_{air} = 0.0214 \times \left(Re_{air}^{\ 0.8} - 100\right) \times Pr_{air}^{\ 0.4} \times \left[1 + \left(D_h / L\right)^{0.66}\right] \quad (27)$$

With conditions : $0.5 \le Pr_{air} \le 1.5,\ 2300 < Re_{air} < 10^6$ et $0 < D_h / L < 1$

- For turbulent flow $\left(Re_{air} > 6000\right)$

$Nu_{air} = 0.023 \times \left(Re_{air}\right)^{0.8} \times \left(Pr_{air}\right)^{0.4}$, (Tan and Charters (1970) empirical correlation). (28)

With : $0.6 \le Pr_{air} \le 160,\ Re_{air} \ge 10000$ et $L/D_h \ge 10$

The Prandtl and Reynolds number is defined by the following relationship [9] :

$$Pr_{air} = \frac{\mu_{air}.Cp_{air}}{\nu_{air}} \text{ et } Re_{air} = \frac{V_{air} D_h}{\nu_{air}}, \text{ avec } D_h = \frac{4\left[\ell \cdot H_c - N_{tube}\,\pi\ D_{ext}/2\ ^2\right]}{2\ \ell + H_c} \quad (29)$$

Where : D_h,ℓ and $H_c$are hydraulic pipe diameter, sensor width and air pipe height respectively.

The thermo-physical characteristics of water are assumed to vary linearly with temperature [5,17,18,19,20] :

– Mass density inkg.m^{-3} :

$$\rho_{wat} = -510.3061 + 15.19367\left(T_{wat}\right) - 5.490006 \times 10^{-2}\left(T_{wat}\right)^2 + 8.538520 \times 10^{-5}\left(T_{wat}\right)^3 - 5.122868 \times 10^{-8}\left(T_{wat}\right)^4 \quad (30)$$

– Specific heat in J.kg^{-1}.K^{-1}:

Regime 1 : $0^{\circ}C < T_{wat} < 137^{\circ}C$

$$Cp_{wat} = \left[\begin{array}{l} 2.13974 - 9.68137 \times 10^{-3}\left(T_{wat}\right) + 2.68536 \times 10^{-5}\left(T_{wat}\right)^2 \\ -2.42139 \times 10^{-8}\left(T_{wat}\right)^3 \end{array}\right] \times 1000 \times 4.1868 \quad (31)$$

Regime 2 : other températures

$$Cp_{wat} = \left[\begin{array}{l} -11.1558 + 7.96443 \times 10^{-2}\left(T_{wat}\right) - 1.74799 \times 10^{-4}\left(T_{wat}\right)^2 \\ +1.29156 \times 10^{-7}\left(T_{wat}\right)^3 \end{array}\right] \times 1000 \times 4.1868 \quad (32)$$

– Thermal conductivity in W.m^{-1}.K^{-1} :

$$\lambda_{wat} = -2.893282 + 3.003312 \times 10^{-2}\left(T_{wat}\right) - 9.604677 \times 10^{-5}\left(T_{wat}\right)^2 + 1.403673 \times 10^{-7}\left(T_{wat}\right)^3 - 8.019830 \times 10^{-11}\left(T_{wat}\right)^4 \quad (33)$$

– Dynamic viscosity inPas :

$$\mu_{wat} = 2.340194 \times 10^{-5} \times 10^{\left(\frac{250.4833}{T_{wat} - 140.0812}\right)} \quad (34)$$

Nusselt number according to flow regime [7,19,20,21,22,23] :

- Forlaminar flow $\left(Re_{wat} < 2300\right)$

$Nu_{wat} = 4.36$,avec $L/D_{int} \gg 50$ (35)

- For transient flow $\left(2300 \le Re_{wat} \le 6000\right)$

$f_d = \left(0.79 \times \ln\left(Re_{wat}\right) - 1.64\right)^{-2}$, where$f_d$is the Darcy-Weisbach friction factor. (37)

$$Nu_{wat} = \frac{\left(f_d/8\right) \times \left(Re_{wat} - 1000\right) \times Pr_{wat}}{1 + 12.7\sqrt{f_d/8}\left(Pr_{wat}^{2/3} - 1\right)}, \text{ (Gnielinski relation).} \quad (38)$$

- For turbulent flow $\left(Re_{wat} > 6000\right)$

$Nu_{wat} = 0.023 \times \left(Re_{wat}\right)^{0.8} \times \left(Pr_{wat}\right)^{0.4}$, (Dittus-Boelterrelationship) (39)

2.3Compound Parabolic Cylindrical Solar Concentrator [1,5,10,21]

The compound parabolic cylindrical concentrator represents an advancement over the conventional parabolic trough design, providing enhanced solar radiation capture and a more uniform energy distribution on the dual-fluid PVT receiver. This improvement reduces thermal hotspots and increases both the thermal and optical efficiency of the system.

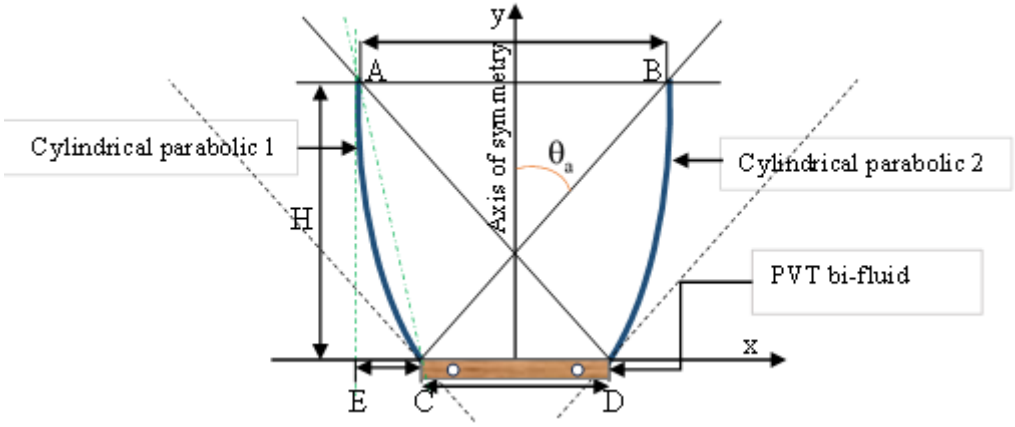

Figure 3:Compound Parabolic Cylindrical Concentrator

❖ **Geometrical considerations**

The concentrator's geometry is characterized by its aperture width, acceptance angle (θ_a) and height. The key dimensional relationships are derived using the following expressions [5,19,22] :

$$\begin{cases} f = \dfrac{CD(1+\sin\theta_a)}{2}; & AB = \dfrac{CD}{\sin(\theta_a)} \\ H = \dfrac{AB+CD}{2.\tan(\theta_a)}; & C_g = \dfrac{AB}{CD} = \dfrac{1}{\sin(\theta_a)} \end{cases} \quad (40)$$

Where :f, AB, CD, H, and C_g are respectively the focal line, entrance pupil width, exit pupil width, height and geometric concentration factor of the reflector.

❖ **Energy concentration (Ce)**

The energy concentration of a solar collector is defined as the ratio between the solar energy incident on the concentrator aperture and the energy actually absorbed by the dual-fluid PVT receiver. It depends on both the optical efficiency and the geometric concentration factor [10,21].

$$C_e = C_g \times \eta_{opt} = C_g \times (\rho_{ccp})^{N_r} \times \eta_{int} \text{ , avec } \eta_{int} = 1 - e^{-C_g} \quad (41)$$

Where: ρ_{ccp} , N_r and η_{int} represent the reflectivity of the mirrors, the average number of reflections a ray undergoes before reaching the dual-fluid PVT and the interception factor.

2.4 Performance of the PVT dual-fluid hybrid collector

The electrical and thermal power outputs of the dual-fluid PVT hybrid solar collector are expressed by the following equations [10,12,14,23]:

$$Q_{élec} = \tau_g.G_i.C.S_{cel}.\eta_{ref}.\exp\left[\beta(T_{cel} - T_{ref})\right], \text{ où } G_i \text{ est l'irradiation solaire globale.} \quad (42)$$

$$Q_{the,wat} = \dot{m}.Cp_{wat}.(T_{wat,out} - T_{wat,int}) \text{ and } Q_{the,air} = \dot{m}.Cp_{air}.(T_{air,out} - T_{air,int}) \quad (43)$$

$$Q_{the,PVT\_bi-fluid} = Q_{the,wat} + Q_{the,air} \quad (44)$$

The electrical and thermal efficiencies of the PVT dual-fluid hybrid solar collector are determined by the following two expressions [14,23,24] :

$$\eta_{elc} = \frac{Q_{elec}}{S_{cel} \cdot G_i \cdot C} \text{ and } \eta_{the,PVT\_bi-fluid} = \frac{Q_{the,PVT\_bi-fluid}}{S_{cel} \cdot G_i \cdot C} \quad (45)$$

The overall efficiency of a dual-fluid PVT is the sum of the thermal efficiency and the thermal efficiency equivalent to the electrical efficiency [24,25,26,27] :

$$\eta_{PVT\_bi-fluid} = \eta_{the} + \eta_{elec,the} \text{ ; with : } \eta_{elec,the} = \frac{\eta_{elec}}{C_f}, \quad (46)$$

Where $C_f$represents the thermal energy conversion factor, with a typical value of 0.38 [28].

2.5Study site

The data used were obtained from the ASECNA meteorological station in Mahajanga, located in the northwestern region of Madagascar (15°43' S, 46°19' E). The Page model was employed to estimate solar irradiation based on insolation data collected between 2010 and 2022.

2.6Electrical characteristics

The polycrystalline silicon photovoltaic collector described in Table 1 has been evaluated to international standards at 1000 $W.m^{-2}$, AM 1.5 and 25°C.

Table 1:Electrical characteristics of a KC200GT photovoltaic module [8,10,29].

Experimental peak power P_{max}	200 W
Voltage at point of maximum power V_{pm}	26.3 V
Current at point of maximum power I_{pm}	7.61 A
Opern circuit voltage V_{oc}	32.9 V
Short-circuit current I_{sc}	8.21 A
Voltage temperature coefficient k_v	–0.123 V/°C
Current temperature coefficient k_i	0.00318 A/°C
Operatin temperature	–40 °C à +85 °C
Numberof cells in série N_s	54
Number of parallel cells N_p	1
Reference efficiency	15 %
Dimension $(L \times l \times h)$	1425 mm × 990 mm × 36 mm

2.7Component characteristics of the dual-fluid hybrid PVT collector

Table 2 shows the characteristics of the various sensor components.

Table 2:Characteristics of the dual-fluid hybrid PVT collector components [10,13,14,23].

Composants / Characteristics	Glass	PV cell	Tedlar	Absorber	Tube	Insulation	Unit
Density	2200	2330	1300	2700	2700	60	$(kg.m^{-3})$
Specific heat	670	836	1400	900	900	700	$(J.kg^{-1}K^{-1})$
Thermal conductivity	0.93	148	0.033	237	237	0.04	$(W.K^{-1}.m^{-1})$
Emissivity	0.88	0.93	0.88	0.04	0.04	0.85	---
Thickness	0.003	0.0003	0.0005	0.005	0.001	0.004	(m)
Absorption coefficient	0.066	0.85	0.5	0.75	0.75	0.066	---
Pipe outside diameter					0.014		(m)
Inside pipe diameter					0.012		(m)

III. Result

3.1 Variation of solar irradiation and ambient temperature in Mahajanga

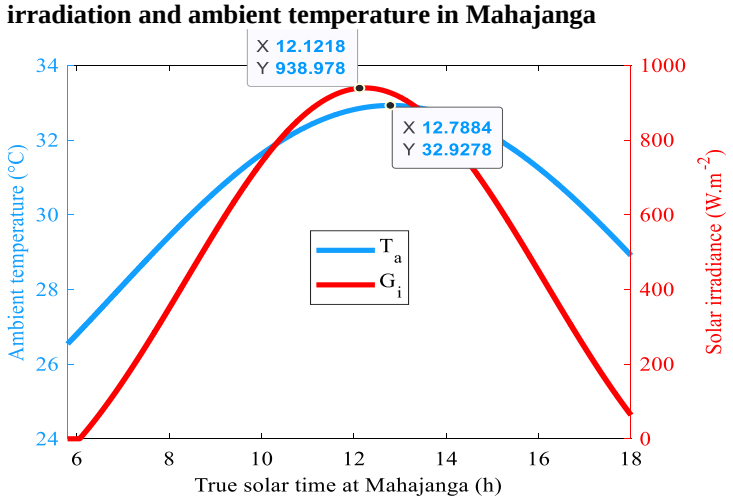

Figure 4: Temporal variation of solar irradiation and ambient temperature in Mahajanga

Figure 4 shows the simulated monthly average variation of solar irradiation and ambient temperature during a typical day of the considered month, based on a 14-year dataset. In Mahajanga, solar irradiation gradually increases in the morning, reaching a peak of 940 W·m⁻² around noon, before decreasing in the afternoon. Ambient temperature varies throughout the day, influenced by the thermal inertia of materials. It reaches its maximum value of 32.92 °C at 12:30 p.m., slightly after the peak in solar irradiation. Morning temperatures are generally lower than those in the evening.

3.2Effect of solar concentration ratio on the energy performance of a dual-fluid CPVT system

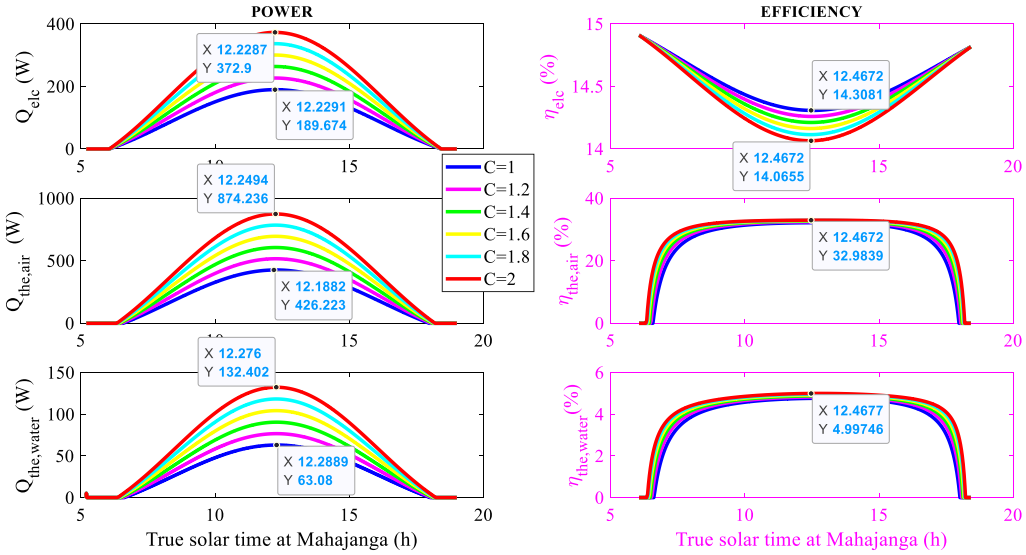

Figure 5: Temporal evolution of the energy efficiency of the dual-fluid CPVT system as a function of solar concentration

The figure illustrates the temporal evolution of thermal and electrical power outputs, as well as the efficiencies of the dual-fluid (water–air) CPVT system, as a function of the solar concentration ratio (C) in Mahajanga. The simulation was conducted using constant geometric and thermal parameters: 22 fins, a fin thickness of 0.003 m, a fin height of 0.02 m, a wind speed of 3 $m.s^{-1}$, and mass flow rates of 0.02 kg·s⁻¹ for both water (total flow) and air.

Increasing the concentration ratio from C = 1 to C = 2 results in a notable enhancement in system performance. The electrical power output (Q_{elc}) increases from 189.7 W at C = 1 to a peak of 372.9 W at C = 2, representing an improvement of approximately 96%. Simultaneously, the thermal power extracted by air

($Q_{the,air}$) rises from 426.2 W to 874.2 W, and that extracted by water ($Q_{the,water}$) from 63.1 W to 132.4 W, indicating a doubling in thermal energy recovery.

Regarding system efficiency, the electrical efficiency (η_{elc})slightly decreases from 14.06% at C = 1 to 14.31% at C = 2, likely due to the heating of photovoltaic cells. In contrast, thermal efficiencies significantly improve: $\eta_{the,air}$reaches 32.98%, and $\eta_{the,water}$reaches 4.99%, suggesting that solar concentration primarily enhances heat recovery. However, the thermal efficiency of the water circuit remains lower than that of air, likely due to the overall cooling effect of the numerous fins on the upper absorber plate, which reduces the internal temperature available for heat transfer to the water flowing in the lower channel.

3.3Effect of fin number on the energy efficiency of a dual-fluid CPVT collector

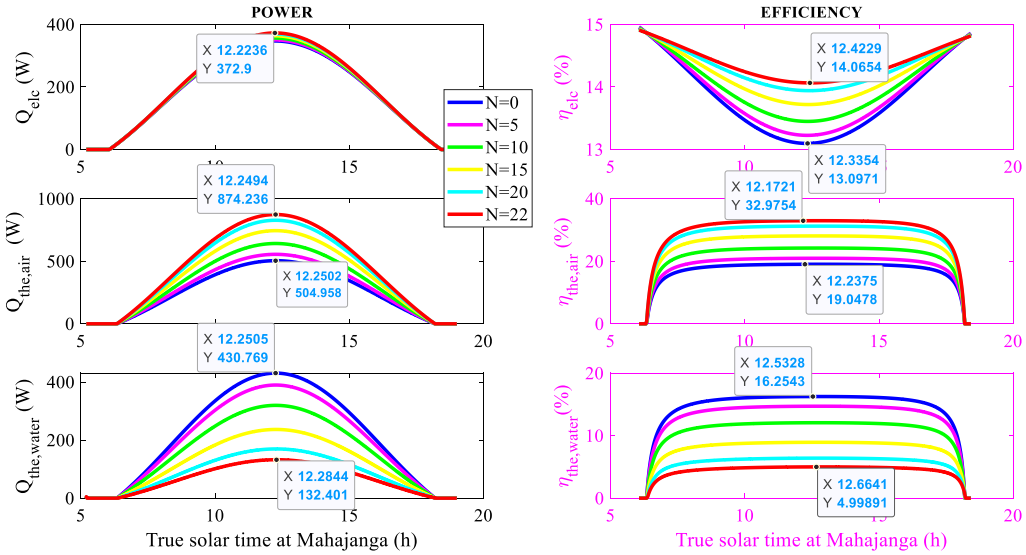

Figure 7: Temporal evolution of the energy efficiency of the dual-fluid CPVT system as a function of the number of fins

La figure 7 Figure 7 illustrates the influence of the number of fins (N) on the electrical and thermal performance of a dual-fluid CPVT system under solar concentration (C = 2). The simulation was conducted with an air layer height of 0.03 m, fin thickness and height of 0.003 m and 0.02 m respectively, a water mass flow rate of 0.004 $kg \cdot s^{-1}$ per tube, and an air mass flow rate of 0.02 $kg \cdot s^{-1}$.

The electrical power output (Q_{elc}) follows the solar irradiation profile, peaking around noon, and is only slightly affected by the number of fins. However, the electrical efficiency improves with increasing N due to enhanced cooling of the photovoltaic cells, which reduces their temperature and thus improves their performance.

Thermally, the heat recovered by air ($Q_{the,air}$) increases with N as a result of improved heat dissipation facilitated by the fins. Conversely, the thermal power extracted by water ($Q_{the,water}$) decreases with N, as the increased cooling of the absorber plate lowers the tube temperature, thereby limiting heat transfer to the water.

Consequently, the thermal efficiency of air ($\eta_{the,air}$) increases with N, while that of water ($\eta_{the,water}$) decreases for the same reason. The addition of fins therefore enhances system cooling and thermal transfer to air, which benefits electrical efficiency but reduces thermal energy recovery by water. A trade-off must be considered to balance these effects and optimize the overall performance of the system.

3.4Effect of fin height on the energy performance of the dual-fluid CPVT system

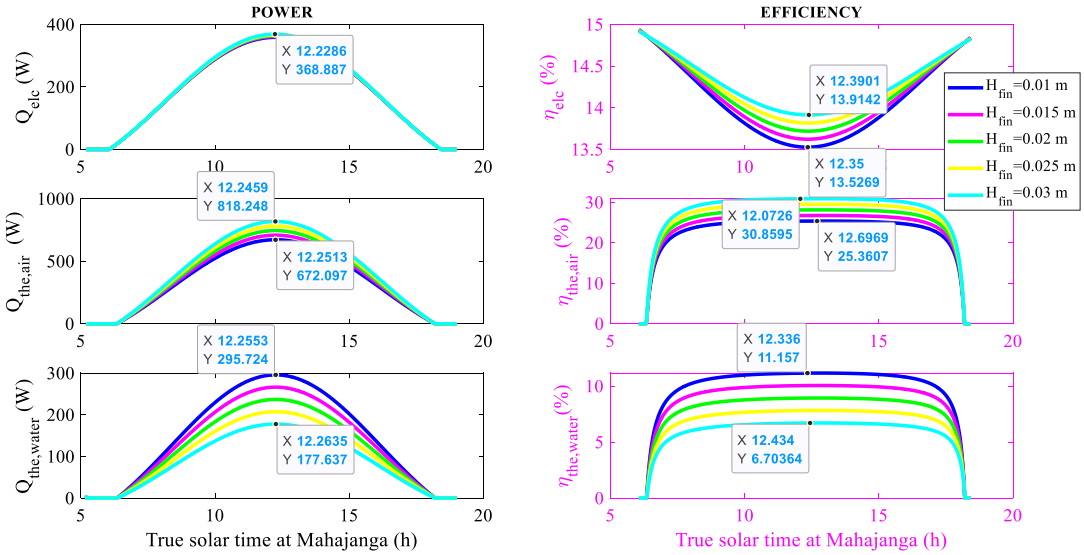

Figure 8: Temporal evolution of the energy efficiency of the dual-fluid CPVT system as a function of fin height.

La Figure 8 illustrates the effect of fin height on the performance of the dual-fluid CPVT system, with the number of fins fixed at 15 and all other parameters kept constant (air channel height, fin thickness, and fluid mass flow rates).

Electrically, the power output remains stable at 368.8 W around noon, while the efficiency improves with increasing fin height due to enhanced heat dissipation.

Thermally, increasing fin height enhances the performance of the air circuit, reaching 818.2 W and an efficiency of 30.9%, due to improved heat exchange. Conversely, water performance decreases, as the increased cooling of the absorber plate and tubes favors heat transfer to the air, thereby reducing the amount of heat absorbed by the water. A lower fin height optimizes the thermal performance of the water circuit, yielding 295.7 W and an efficiency of 11.2%.

3.5Effect of fin thickness on the energy performance of the dual-fluid CPVT system

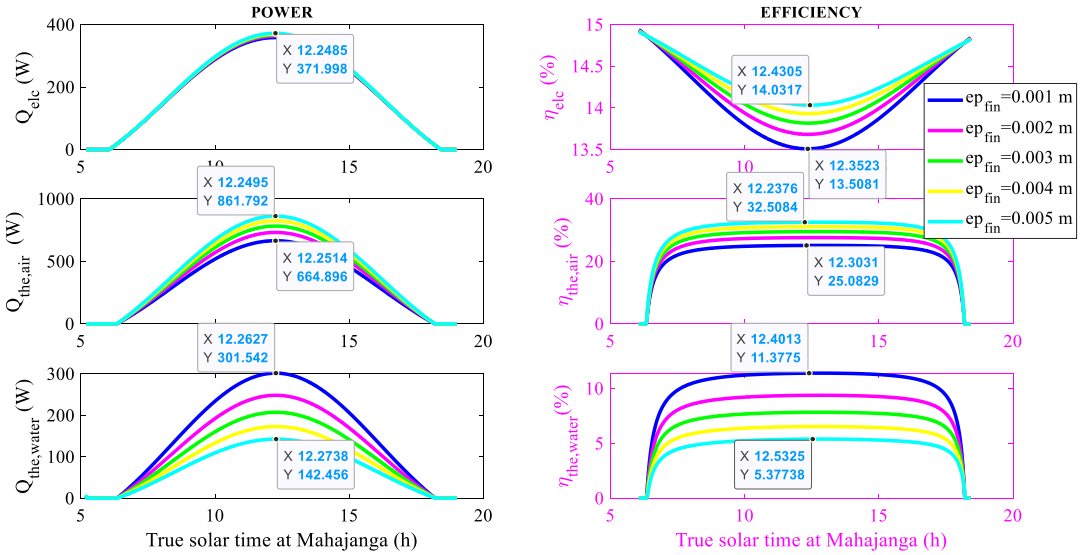

Figure 9: Temporal evolution of the energy efficiency of the dual-fluid CPVT system as a function of fin thickness

Figure 9 illustrates the effect of fin thickness on the energy performance of the dual-fluid CPVT system, with trends similar to those observed for fin height.

An increase in fin thickness significantly enhances electrical efficiency, which reaches 14%, as well as the thermal performance of the air circuit, with an efficiency of 32.5%. This improvement is attributed to a larger contact surface, which promotes better heat transfer and more effective cooling.

However, the increased heat dissipation to air lowers the temperature of the absorber plate and tubes, reducing the heat absorption capacity of the water circuit and negatively affecting its thermal performance.Therefore, increasing both fin height and thickness improves system cooling, benefiting electrical and air-side thermal efficiencies, but to the detriment of water-side thermal performance.

3.6Effect of water and air mass flow rates on the energy performance of the dual-fluid CPVT System

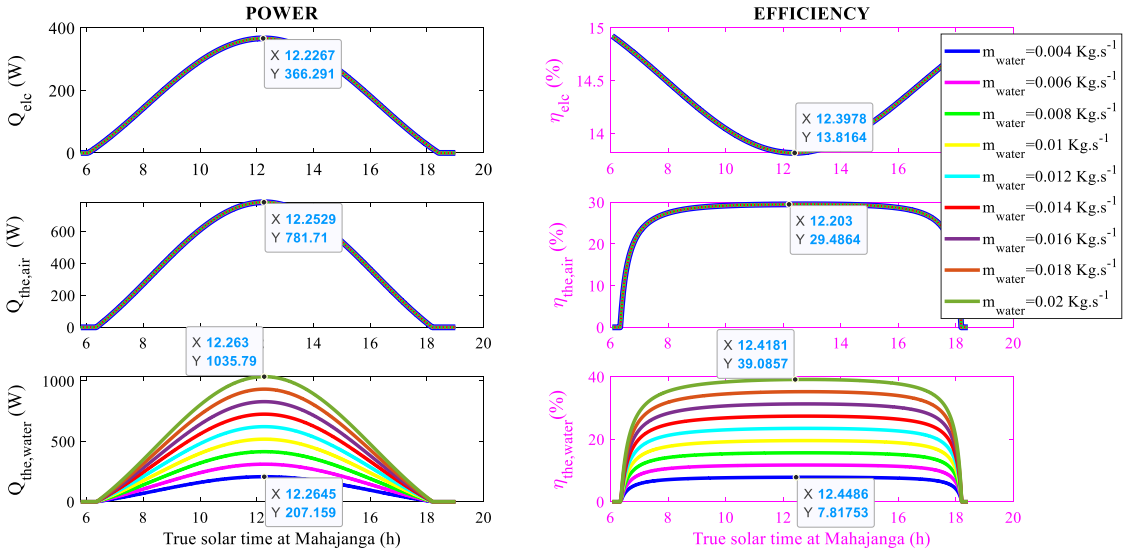

Figure 10 : Temporal evolution of the energy efficiency of the dual-fluid CPVT system as a function of water mass flow rate

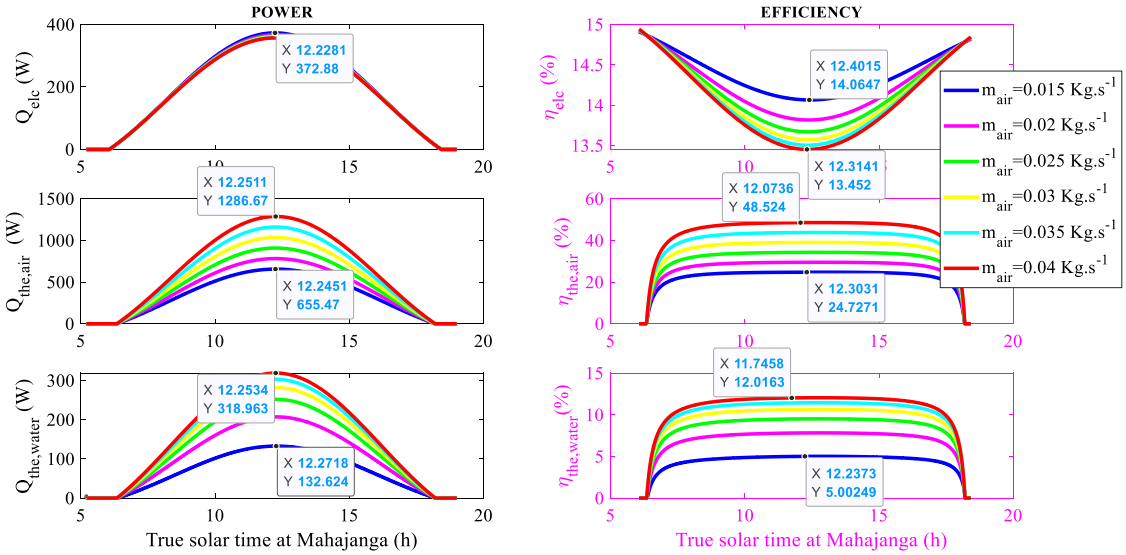

Figure 11 : Temporal evolution of the energy efficiency of the dual-fluid CPVT system as a function of air mass flow rate

Figure 10 illustrates the effect of the water mass flow rate on the energy performance of the dual-fluid CPVT system, with a fixed air mass flow rate of 0.02 kg.s^{-1}. The results show that variations in water mass flow rate do not affect the electrical performance (Q_{elc}, η_{elc}) or the thermal performance of the air circuit ($Q_{the,air}$, $\eta_{the,air}$), as the corresponding curves remain unchanged. However, the water flow rate directly influences the thermal performance of the water circuit ($Q_{the,water}$, $\eta_{the,water}$): increasing the water mass flow rate enhances the thermal energy recovery and improves the thermal efficiency. Therefore, optimizing the water mass flow rate can maximize heat recovery without impacting the system's electrical or air-side thermal performance.

Figure 11 shows the influence of air mass flow rate on the energy performance of the dual-fluid CPVT system, with a fixed water mass flow rate of 0.004 kg.s^{-1}per tube. The electrical power output remains steady at approximately 372.9 W, while electrical efficiency decreases with increasing air flow rate, reaching around 14% at 0.015 kg.s^{-1}before gradually declining. In contrast, the thermal performance of the heat transfer fluids (air and water) improves with higher air flow rates, indicating more effective heat exchange. This effect is particularly significant for the water circuit, whose thermal efficiency increases notably. Thus, air mass flow rate has a major impact on the system's thermal performance, while its influence on electrical performance remains limited.

3.7Maximized energy efficiency of the dual-fluid CPVT System

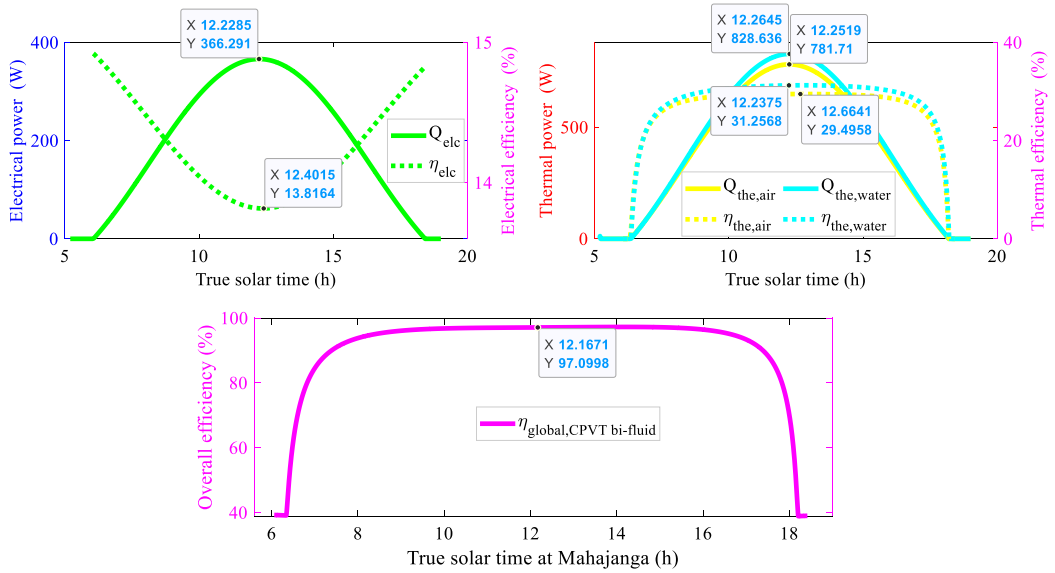

Figure 12 : Energy efficiency of the dual-fluid CPVT system

Figure 12 illustrates the outstanding energy efficiency of the dual-fluid CPVT system under optimized operating conditions. The selected moderate configuration under solar concentration (C = 2) includes: 15 fins, 5 tubes, a fin thickness of 0.003 m, a fin height of 0.025 m, an air channel height of 0.03 m, a spacing of 0.046 m between fins and tubes, a water mass flow rate of 0.016 kg.s^{-1} (per tube), and an air mass flow rate of 0.022 kg.s^{-1}.

These results reveal an excellent balance between electrical and thermal outputs in the hybrid dual-fluid CPVT system. Throughout the solar day, the system's performance remains optimized, demonstrating an effective synergy between air and water as heat transfer fluids.

From an electrical standpoint, the generated power peaks at 366.3 W around noon, with an electrical efficiency of 13.8%. This efficiency remains relatively stable during periods of high solar irradiation, indicating good photovoltaic conversion under moderate concentration.

Thermally, the performances are also well balanced. The thermal power recovered by air reaches a maximum of 781.7 W, while that of water rises to 828.6 W. The associated thermal efficiencies show good stability between 9:00 AM and 4:00 PM, reflecting effective heat dissipation throughout this period. The thermal efficiency of the air circuit reaches 29.5%, while that of the water circuit is 31.2%.

Finally, the optimized global energy efficiency of the dual-fluid CPVT system reaches 97%, demonstrating a highly effective energy conversion. These results highlight the potential of such a system for combined applications, particularly for simultaneous electricity and heat production, suitable for diverse uses such as powering electrical equipment or meeting thermal demands like drying and domestic hot water production.

IV. Discussion And Conclusion

This study focused on the performance optimization of a hybrid dual-fluid (air–water) photovoltaic-thermal system coupled with a compound parabolic cylindrical concentrator (CPVT). The objective was to maximize the utilization of incident solar energy by balancing electrical and thermal outputs, primarily through fine control of the cooling conditions.

The system enables the cogeneration of electricity, hot water, and hot air. The integration of fins within the air channel proved effective in enhancing heat transfer, thereby maintaining moderate photovoltaic cell

temperatures and improving their efficiency. Although beneficial to the electrical output, this configuration leads to a relative decrease in the thermal recovery on the water side. Moreover, the thermophysical characteristics of the heat transfer fluids, particularly their respective mass flow rates, were shown to be key parameters influencing the system's thermal behavior.

The parametric analysis revealed the significant influence of several factors on the dual-fluid CPVT system performance, including the solar concentration ratio, the fin geometry (number, height, and thickness), and the mass flow rates of air and water. An optimal configuration was identified through numerical simulation using MATLAB and the Runge-Kutta solution method. This optimal setup included: 15 fins, 5 tubes, fin thickness of 0.003 m, fin height of 0.025 m, a spacing of 0.046 m between fins and tubes, a water mass flow rate of 0.016 $kg.s^{-1}$ per tube (0.08 $kg.s^{-1}$ total), an air mass flow rate of 0.022 $kg.s^{-1}$, and an air channel height of 0.03 m. The system yielded the following performance:

- Electrical output : peak power of 366.3 W around noon, with an electrical efficiency of 13.8% and cell temperature limited to 45.5 °C under concentration.
- .Thermal output : 828.6 W from the water loop at 45.28 °C ($\eta_{the,water}$= 31.2%), and 781.7 W from the air loop at 70.1 °C ($\eta_{the,air}$= 29.5%) under concentration.
- Overallenergyefficiency : up to 97%, highlighting the system's potential for high-efficiency solar cogeneration.

These findings confirm that the dual-fluid CPVT system, through optimized geometry and thermal conditions, offers a viable solution for integrated solar energy harvesting. Its versatility makes it suitable for applications requiring both electricity and heat, such as solar-assisted drying, domestic hot water production, or industrial process heating.

Future developments will focus on the intelligent control of the system by implementing an adaptive MPPT (Maximum Power Point Tracking) algorithm based on artificial intelligence. This will allow for real-time optimization of both electrical and thermal outputs under dynamically changing environmental conditions, further increasing the reliability, autonomy, and efficiency of the CPVT system.

References

[1]. Olivier FARGES, 'Conception optimale de centrales solaires à concentration: application au centrales à tour et aux installations 'beam down'. Thèse, Université de Toulouse, 2014.

[2]. Tripathi, Rohit, G.N. Tiwari, 2017. 'Annual performance evaluation (energy and exergy) of fully covered concentrated photovoltaic thermal (PVT) water collector: an experimental validation'. Sol. Energy 146, 180–190.

[3]. Deepali Atheaya, A. Tiwari, G.N. Tiwari., 2016. 'Experimental validation of a fully covered photovoltaic thermal compound parabolic concentrator system'. Engineering Science and Technology an International Journal · July 2016.

[4]. Ahed Hameed Jaaz, Husam A. H., Kamaruzzaman S.,Abdul Amir H. K., Tayser Sumer G. and Ahmed A. AlAmiery , 'Outdoor Performance Analysis of a Photovoltaic Thermal (PVT) Collector with jet Impingement and Compound Parabolic Concentrator (CPC)', Materials 2017, 10, 888.

[5]. MEKADEM Hafsa et Mellouki H., 'Etude paramétrique d'un capteur hybride doté d'un concentateur parabolique composé (PVT-CPC)', Mémoire, Université Ahmed Draia-Adrar, 2022.

[6]. Wenzhi Cui, Long Zhao, Wei Wu, 2010. 'Energy Efficiency of a Quasi CPC Concentrating Solar PV/T System', IMECE2010

[7]. TABET Ismail. 'Etude, Réalisation et simulation d'un capteur solaire', thèse, Université des freres mentouri constantine, 2016.

[8]. PASERA Joanès Keneddy, HARITHI BEN et DONA Victorien Bruno, « Optimizing the energy performance of a hybrid PVT air collector with Parabolic trough concentrator and Heliostat», IJARIIE-ISSN(O)-2395-4396, Vol-10 Issue-5 2024

[9]. PASERA Joanès Keneddy, HARITHI BEN et DONA Victorien Bruno, 'Thermal efficiency of the Photovoltaic-Thermal air-coupled Parabolic through-Heliostat Concentrator (PVT-CCPH)', IJARIIE-ISSN(O)-2395-4396, Vol-10 Issue-6 2024.

[10]. PASERA Joanès Keneddy, HARITHI BEN et DONA Victorien Bruno, 'Performance Analysis of a Dual-Fluid CPVT Solar Concentrator (Water and Air)', IJERD e-ISSN: 2278-067X, p-ISSN:2278-800X, Vol 21, Issue 5 (May 2025), PP 116-129.

[11]. El-YAHYAOUI Sara., 'Photovolta¨ıque à concentration : optimisation de l'´étage secondaire', Thèse en cotutelle, Université Sidi Mohamed Ben Abdellah & Université de Lorraine, le 26 mars 2021.

[12]. TOUAFEK Khaled, 'Contribution à l'étude et à la conception d'un système énergétique utilisant des capteurs hybrides photovoltaïques thermiques', Thesis, Ecole Normale Polytechnique ENP, Algeria, 2010.

[13]. S. Ben Mabrouk, 'Etude et Simulation d'un Capteur hybride Photovoltaique Thermique à air', University of Tunis El Manar, Researchgate, 2016.

[14]. Oussama El Manssouri, Chaimae E. F, Bekky H et al., 'Mass Flow Rates Effect on the Performance of PV/T Bifluid Hybride Collector (Single and Simultaneous Modes)'.,2021, in Electrical Engineering 681,

[15]. Khelifa Abdelkrim., 'Contribution à la conception et modélisation d'un capteur solaire hybride photovoltaïque thermique PVT'., Thèse, Univertsité Hadj Lakhdar de Batna, 2017.

[16]. Incropera, F.P.; DeWitt, D.P. 'Fundamentals of Heat and Mass Transfer', 6th ed.; John Wiley & Sons, Inc.: Hoboken, NJ, USA, 2007.

[17]. GHELLAB Amel, 'Modélisation et optimisation des capteurs solaires hybrides', Thèse, Université des frères Mentours Constantine, 2018

[18]. AKERMI Mustapha, 'Modelisation, simulation et analyse de comportement d'un capteur solaire plan à eau pour différents sites en ALGERIE'., These, Université Abou-bekr belkaid-Tlemcen, 2019.

[19]. GUENDOUZI Seyf eddine et LOUNIS Ibrahim., 'Performances d'un Capteur Hybride PVT/Bifluide', Memoire, Université de JIJEL, 2014.

[20]. Bourouaiah Yassine, Kimouche Fouaz., 'Etude numérique des performance d'un capteur solaire plan à eau'., Memoire, Université Mohamed Seddik Ben Yahia – Jijel, 2021

[21]. BOUHOREIRA Y. and GANA L. 'Etude de l'effet des paramètres sur les performances d'un collecteur solaire cylindro parabolique', mémoire, Université Kasdi Merbah Ouargla, 24-06-2018.
[22]. René RAUD, Chapidtre I DOSSIER DE CALCULS-soleil-vapeur,
[23]. Oussama El Manssouri, B. Hajji, Giuseppe M.T, Antonio G. and Stefano A., 'Electrical and Thermal Performances of Bi-Fluid PV/Thermal Collectors'. Energies 2021, 14, 1633.
[24]. M.Y. Othman, S.A. Hamid et al., Performance analysis of PV/T Combi with water and air heating system: An experimental study. Renewable Energy 86 (2016) 716e722
[25]. Nurul Shahirah Rukman, Ahmad F. et al., Bi-fluid cooling effet on electrical characteristics of flexible photovoltaic panel., Journal of Mechatronics, Electrical Power, and Vehicular Technology 12 (2021) 51 -56
[26]. Mohammad Sardarabadi, Mohammad P., Experimental and numerical study of metal-oxides/water nanofluids as coolant in photovoltaic thermal systems (PVT)., Solar Energy Materials & Solar Cells 157 (2016) 533–542
[27]. Hasila Jarimi, Mohd Nazari A. B., et al., Bi-fluid photovoltaic/thermal (PV/T) solar collector: experimental validation of a 2-D theoretical model., Renewable Energy 85 (2016) 1052 e1067
[28]. Juwel Chandra Mojumder, Wen Tong C., et al., An experimental investigation on performance analysis of air type photovoltaic thermal collector system integrated with cooling fins design.
[29]. BELKACEM Mourad, 'Etude et optimisation du transfer d'énergie électrique en conversion photovoltaïque par la recherche du point de puissance maximal (MPPT)', Mémoire, Université Abou Belkaid de Tlemcen, 2015.